Journal of Catalysis **190,** 215–227 (2000)
doi:10.1006/jcat.1999.2740, available online at http://www.idealibrary.com on IDEAL®

Selective Oxidation of Ethane to Acetaldehyde and Acrolein over Silica-Supported Vanadium Catalysts Using Oxygen as Oxidant

Zhen Zhao,*,† Yusuke Yamada,* Yonghong Teng,† Atsushi Ueda,*
Kiyoharu Nakagawa,‡ and Tetsuhiko Kobayashi[1,]*

*Osaka National Research Institute, AIST-MITI, Ikeda, Osaka 563-8577, Japan; †Research Institute of Innovative Technology for the Earth, Kizu-cho, Kyoto 619-0292, Japan; and ‡Department of Chemical Engineering, Kansai University, Suita, Osaka 564-8680, Japan

Received March 4, 1999; revised October 15, 1999; accepted October 22, 1999

The oxidation of ethane by oxygen was studied over silica catalysts supporting different amounts of vanadium with and without cesium. Three different catalytic properties of the product selectivity were observed, aldehyde formation, oxidative dehydrogenation (ODH), and combustion, depending upon the vanadium loading amount and the presence or the absence of cesium. A very low loading of vanadium (V:Si = 0.02–0.1 at.%) and the addition of Cs (Cs:Si = 1 at.%) on silica were found to be important for the formation of aldehyde. Not only acetaldehyde but also acrolein were observed in the aldehyde formation from ethane. On the other hand, catalysts with medium and high vanadium loadings (V:Si = 0.5–20 at.%) gave a dehydrogenated product, ethene, when Cs was not added to the catalysts. The addition of cesium to the catalysts with medium and high vanadium loadings changed the catalytic property from ODH to combustion. The different types of vanadyl species were identified by UV–visible and IR measurements in samples with different vanadium loadings. It was estimated that isolated vanadyl species with tetrahedral coordination, which were found mainly on the catalysts with vanadium loading lower than 0.5 at.%, became the active site for the aldehyde formation through the interaction with Cs. As a plausible reaction path giving acrolein from ethane, cesium-catalyzed cross-condensation between acetaldehyde and formaldehyde, formed in the reaction, was proposed. Polymeric vanadyl species with octahedral coordination and vanadium–oxygen clusters with dioxo tetrahedral coordination were detected in the samples with medium (0.5–5.0 at.%) and high (10 and 20 at.%) vanadium loadings, respectively. Both species show the ODH catalytic property without cesium, but they bring about a deep oxidation of ethane if cesium is added to the catalysts.

Key Words: **selective oxidation of ethane; silica-supported vanadium; loading of vanadium; acetaldehyde; acrolein; isolated vanadyl species; oxygen.**

1. INTRODUCTION

Direct conversion of light alkanes on useful oxygenates is a big challenge in catalyst research on the effective utilization of natural gas. Vanadium and molybdenum are widely used as common and indispensable catalytic components for the selective oxidation reaction (SOR) of light alkanes (1–4). In the case of ethane oxidation, however, oxygenate formation is much more difficult than oxidative dehydrogenation (ODH) of ethane. Iwamoto *et al.* (5) reported that a trace amount of acetaldehyde was formed in the ODH of ethane by N_2O over silica catalysts supporting V_2O_5 or MoO_3. Oyama and Somorjai (6, 7) have also reported that a small amount of acetaldehyde was detected in the ODH of ethane by oxygen over pure silica as well as silica-supported vanadium oxides. Erdohelyi and Solymosi (8–13) have published a series of reports concerning the SOR of ethane over silica-supported alkali metal vanadate and molybdate. They concluded that N_2O is a better oxidant than oxygen for acetaldehyde formation over these catalysts.

The comparative results on vanadium-containing catalysts for the SOR of ethane to acetaldehyde, reported in the literature, are listed in Table 1. Even when N_2O was used as the selective oxidant, an acetaldehyde yield higher than 2% was difficult to obtain. In most cases, loading amounts of vanadium or molybdenum on the catalysts were larger than 1 wt% of the supports.

Although there are many reports concerning the active species in the vanadium-supported catalysts for the SOR of alkane, most of them have focused on ODH, and there are very few reports on oxygenate formation, especially from ethane and propane. Moreover, even for the ODH of alkanes, there are some discrepancies about the vanadium active species (4).

On the one hand, the isolated or well-dispersed vanadyl species have been proposed as active sites for ODH of alkanes (1, 2, 14–17). Kung *et al.* (2, 15) have studied the oxidation of butane over silica- and alumina-supported vanadium pentoxide catalysts with different loadings. LeBars *et al.* (16) have also investigated the ODH of ethane over silica catalysts with different vanadium loadings. In both investigations, the catalysts with lower vanadium loadings

[1] To whom correspondence should be addressed. Fax: 81-727-51-9630. E-mail: kobayashi@onri.go.jp.

0021-9517/00 $35.00

TABLE 1

Comparison of Vanadium Oxide Supported on SiO_2 Reported in the Literature for Ethane Oxidation to Acetaldehyde

Catalyst	Loading of V (wt%)	Reactant gases (1 atm)	Reaction temperature (°C)	Ethane conversion (%)	TOF of ethane consumption (10^{-3} s^{-1})	Ethene selectivity (%)	Acetaldehyde selectivity (%)	Ref.
V_2O_5/SiO_2	4.2	C_2H_6:N_2O:H_2O:He 10.1:20.1:20.2:50.8	550	16.6	—	57.3	1.3	9
KVO_3/SiO_2	2.0	C_2H_6:N_2O:H_2O:He	550	7.7	—	20.7	22.1	13
$K–V_2O_5/SiO_2$	2.0	20:40:20:20	550	3.2	—	14.3	15.0	
V_2O_5/SiO_2	2.0	C_2H_6:N_2O:H_2O:He	550	6.9	2.04			16
$LiVO_3/SiO_2$	2.0	20:40:20:20	550	4.5	5.06			
$NaVO_3/SiO_2$	2.0		550	11.3	42.09			
KVO_3/SiO_2	2.0		550	9.2	17.14			
$RbVO_3/SiO_2$	2.0		550	6.5	14.37			
$CsVO_3/SiO_2$	2.0		550	7.0	25.22			
V_2O_5/SiO_2	3.5	C_2H_6:O_2:H_2O:He	527	0.6	2.2	63.0	12	10
		13:28:10:50	552	1.8	15.0	57.0	11	
V_2O_5/SiO_2	7.7	C_2H_6:O_2:H_2O:He 13:28:10:50	497	0.20	1.1	68.0	17	11

displayed essentially higher selectivity for alkene than that of the bulk V_2O_5. Trifiro and co-workers (1, 17, 18) have found a very high selectivity for the propane ODH on the catalysts having atomically dispersed vanadium ions inside a matrix, such as zeolites and zeolitic compounds.

On the other hand, some researchers have claimed that polymeric vanadyl species and bulk V_2O_5 are active sites for the ODH of hydrocarbons (19–22). Khodakov *et al.* (21, 22) have studied the effects of the vanadium loading and the support on propane ODH. They have pointed out that a support surface that is predominantly covered with polyvanadate structures or small V_2O_5 clusters containing V–O–V or V=O linkages leads to a high oxidative dehydrogenation rate and a high selectivity.

Oyama and Somorjai (6, 7) found that ethane ODH occurs with high selectivity over silica with high vanadium loadings in which vanadium oxide nucleates into small V_2O_5 crystallites, of size <4 nm, but identical to bulk V_2O_5. The formation of CO_x takes place faster on low-loading catalysts. They concluded that the selective reactions that form ethene and acetaldehyde are structure-insensitive, while the reaction to form CO_x is structure-sensitive, based on the study of turnover frequency (TOF) and product distribution.

Recently, Wachs and Weckhuysen (23) published a review regarding the structure and reactivity of surface vanadium species on oxide supports. The following considerations about the active vanadium species are proposed. The surface vanadia species of dehydrated V^{5+} appears to be the predominant and active sites for the hydrocarbon SOR. The terminal V=O bond does not appear to influence critically the catalytic properties of the surface vanadia species during the SOR. The bridging V–O–V bond also does not affect many oxidation reactions, but for those reactions that may be influenced by this bridging bond the TOF may increase only by as much as 1 order of magnitude. The bridging V–O–support bond, however, appears to be most important since its properties can change the TOF for the hydrocarbon SOR by as much as 4 orders of magnitude.

In our previous work, Kobayashi *et al.* (24, 25) found that a very small amount of iron supported on SiO_2 (Fe:Si = 5:10,000 in atomic ratio) can catalyze the methane SOR by oxygen to formaldehyde. It has been pointed out that not iron oxide clusters but tetrahedrally coordinated Fe^{3+}, isolated in the silica network, plays an important role in the formaldehyde formation (25). Recently, Teng and Kobayashi (26, 27) reported a large promotion effect of K^+ on the aldehyde formation from propane and oxygen over Fe/SiO_2. A similar promotion effect is also observed with the addition of Rb or Cs to the catalysts. Isolated Fe^{3+} species on silica are again indispensable for the aldehyde formation from propane in the alkali-promoted catalysts (26, 27), while the iron oxide clusters are active for ODH and combustion. Although Cs^+ was the less advantageous promoter in alkali molybdate catalysts (13) for the acetaldehyde formation from ethane and N_2O, Cs was the most effective element for the silica catalysts supporting alkali vanadates to give acetaldehyde (12). These findings encouraged us to investigate the possibility of oxygenate formation from ethane and oxygen over catalysts having isolated vanadium site and Cs as the promoter.

In the work described in this paper, the oxidation of ethane by oxygen was studied over silica catalysts with different vanadium loading amounts. Depending on the vanadium loading amount and the presence or the absence of Cs, the catalysts were classified into three types: for

aldehyde formation, for ODH, and for combustion. The different types of vanadyl species were identified by UV–visible and IR measurements in samples with different vanadium loadings. The active vanadyl species for aldehyde formation, for ethane ODH, and for deep oxidation were assigned by correlating the catalytic results and vanadyl species characterization. In addition, not only acetaldehyde but also acrolein were detected in the aldehyde formation from ethane. Possible reaction pathways to give acrolein from ethane were also proposed.

2. EXPERIMENTAL

2.1. Catalyst Preparation

All catalysts were prepared by the impregnation method. V/SiO_2 catalysts were prepared by impregnation of SiO_2 powder with an aqueous solution of ammonium vanadate, followed by drying at 80°C in an oven for 10 h and then calcination at 700°C for 6 h. It should be noted that it is difficult to dissolve a large amount of ammonium vanadate in water. Therefore, for the samples with very high loadings of vanadium (10 and 20 at.%), some amount of oxalic acid 2-hydrate was added to allow the formation of a complex that would increase the solubility in water. Cesium-modified V/SiO_2 catalysts were prepared by a two-step impregnation method. First, V/SiO_2 samples were obtained as shown above. Second, the V/SiO_2 samples obtained were impregnated with cesium nitrate aqueous solution, dried, and calcined under the same conditions as used for the first impregnation step.

2.2. Activity Measurement

A fixed-bed flow reactor (quartz tube, 6-mm i.d.) was used at atmospheric pressure for the catalytic activity measurements. A 600 mg catalyst was placed in the middle of the reactor tube with quartz wool. Space in the reactor (pre- and postheating zones) was filled with quartz sand to reduce the effect of autooxidation of the substrate and product in the gas phase. A reaction gas mixture consisting of 75 vol% of C_2H_6 and 25 vol% of O_2 was passed through the catalyst bed at a flow rate of 30 ml min^{-1}. Products were analyzed by gas chromatography using a flame ionization detector with a Porapak-Q column (26, 27). The conditions for the activity measurement of ethylene oxidation were same as those for ethane oxidation. The measuring conditions for the oxidation of C_3H_6 or C_3H_8 were almost same as those in ethane oxidation, except for the reaction gas mixture containing 20 vol% of C_3H_6 or C_3H_8, 16 vol% of O_2, and 64 vol% of N_2 at a flow rate of 100 ml $\cdot$ min^{-1}. The ethanol oxidation reaction was carried out in same flow reactor and analyzed by using the same method of ethane oxidation. The mixture of C_2H_5OH, N_2, and O_2 was introduced into the reactor after mixing gas (N_2:O_2 = 3:1, 30 ml min^{-1}) was bubbled through absolute ethanol.

2.3. Characterization of Catalysts

UV–vis absorption spectra of the samples were measured with a spectrophotometer equipped with a multichannel photodetector (MCPD 2000, Otsuka Electric Co.). SiO_2 was used as a reference sample. IR spectra were recorded on a Nicolet FT-IR 205. The resolution was set at 4 cm^{-1}. The sample was prepared as a KBr pellet. All the samples were pretreated at 200°C for 2 h before making the disks. Electron spin resonance (ESR) of the samples was measured in the X-band region by using a spectrometer (ESP-300E, Bruker) at liquid nitrogen temperature (−196°C). Each sample (100 mg) was placed in a quartz tube in the solid state. Specific surface areas were determined by the BET single-point method using a surface area analyzer (Quantachrom, Jr.).

3. RESULTS

3.1. Activity and Selectivity Measurements

The oxidation of ethane was conducted over silica catalysts with and without vanadium (V:Si = 0.1 at.%) and cesium (Cs:Si = 1 at.%). Figure 1 shows the ethane conversion as a function of the reaction temperature. Almost no reaction in the empty quartz tube was detected when reaction temperatures did not exceed 500°C. The catalyst supporting both vanadium and cesium afforded an appreciably high ethane conversion, which is about 10 times higher than those on the other catalysts at 500°C.

Figure 2 shows the total selectivity toward aldehydes on the silica catalysts with and without V and Cs as a function of

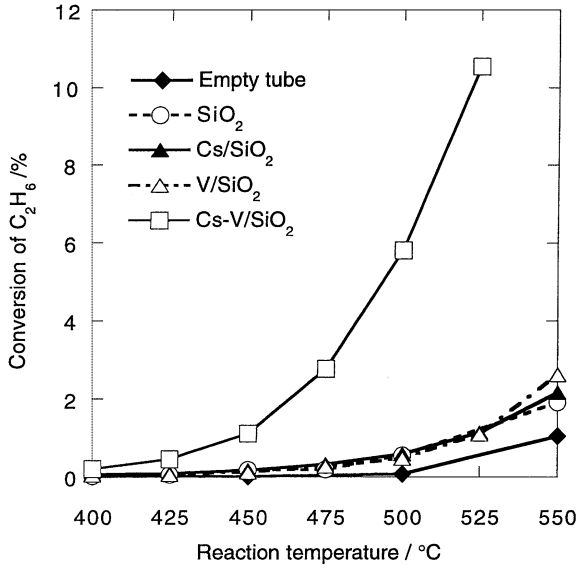

FIG. 1. Ethane conversion over SiO_2, Cs/SiO_2 (Cs:Si = 1:100), V/SiO_2 (V:Si = 0.1:100), and $Cs–V/SiO_2$ (Cs:V:Si = 1:0.1:100) as a function of reaction temperature. Space velocity, 3000 ml g^{-1} h^{-1}; C_2H_6:O_2 = 3:1.

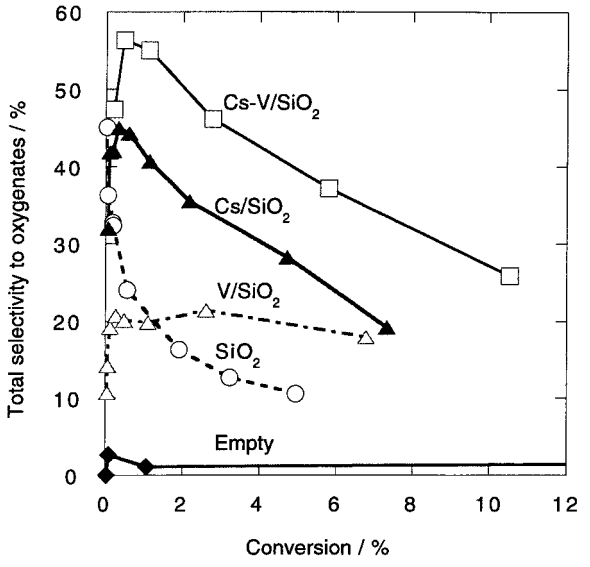

FIG. 2. Total selectivity for aldehydes over SiO_2, Cs/SiO_2 (Cs:Si = 1:100), V/SiO_2 (V:Si = 0.1:100), and $Cs–V/SiO_2$ (Cs:V:Si = 1:0.1:100) as a function of ethane conversion. Space velocity, 3000 ml g^{-1} h^{-1}; C_2H_6:O_2 = 3:1; reaction temperatures, 400–600°C.

the ethane conversion. Different ethane conversions were obtained here by changing the reaction temperature from 400 to 600°C at a fixed space velocity of 3000 ml g^{-1} h^{-1}. As reported by Oyama and Somorjai (6, 7), pure silica and silica-supported vanadium gave aldehydes with small selectivities. The presence of both vanadium and cesium on silica was found to be very effective for aldehyde formation from ethane and oxygen as well as for high ethane conversion (Fig. 1). The addition of only Cs to silica also brought about an improvement in the aldehyde selectivity, but not an improvement in the conversion. Three kinds of reactions, combustion to CO_x, oxidative dehydrogenation (ODH) to ethene, and formation of aldehydes, took place in parallel on the tested silica-supported catalysts.

Figure 3 shows the ethane conversion and the product selectivities of the $Cs–V/SiO_2$ (Cs:V:Si = 1:0.1:100) catalyst as a function of the reciprocal space velocity (i.e., contact time) at 500°C. The ethane conversion increases in proportion to the increase in contact time (i.e., reciprocal flow rate). A drastic change in the product distribution was observed in the aldehyde formation with contact time. Not only acetaldehyde and formaldehyde but also acrolein were detected as the products of the ethane oxidation. Relatively good selectivity for acetaldehyde was observed at a low contact time. The formaldehyde selectivity afforded a similar transformation. In contrast to these transformations, the selectivity for acrolein appreciably increased with contact time, reached a maximum, and then decreased at longer contact times.

The durability of the $Cs–V/SiO_2$ (1:0.1:100) catalysts for aldehyde formation was tested as a function of time on stream, and the results are shown in Fig. 4. Although the total time of the test was about 27 h, no degradation as well as no change in the product distribution was observed. Also, no visual change in the original white color of the catalyst was noticeable after the durability test.

3.2. Effect of Vanadium Loading on the Catalytic Performance of V/SiO_2 (V:Si = x:100) and $Cs–V/SiO_2$ (Cs:V:Si = 1:x:100)

Figure 5 shows the effect of the vanadium loading on the product distribution and ethane conversion at 475°C over V/SiO_2 (a) and $Cs–V/SiO_2$ (b), respectively. In the cesium-free catalysts (Fig. 5a), vanadium addition up to 0.1 at.% on silica did not bring about much enhancement of the original silica activity. An enhancement of the conversion was distinct with and roughly in proportion to the increasing vanadium loadings from 0.1 to 5 at.%. An enhancement of

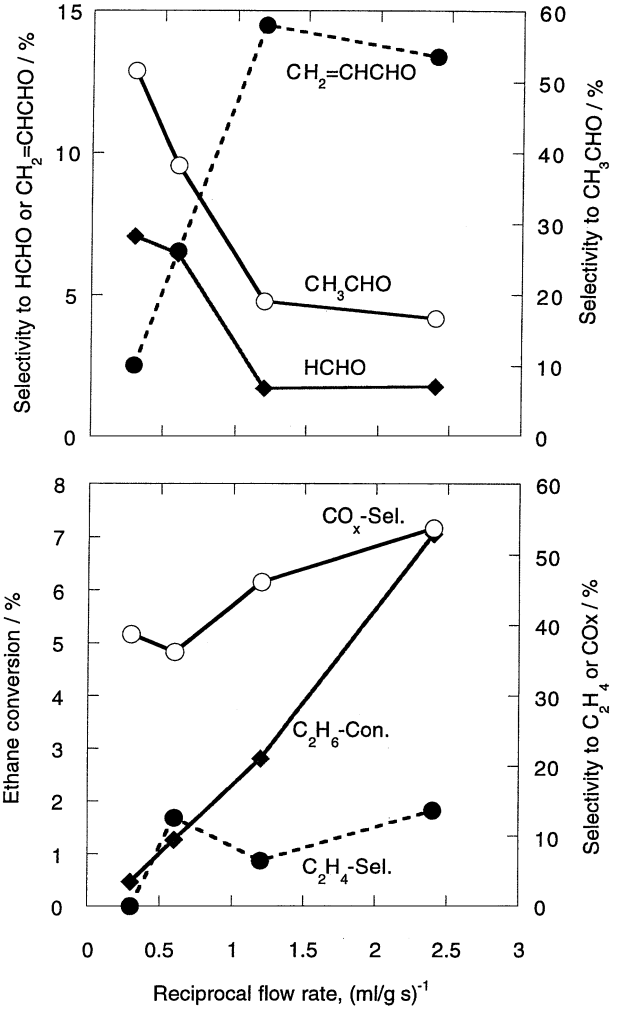

FIG. 3. Ethane conversions and product selectivities over $Cs–V/SiO_2$ (Cs:V:Si = 1:0.1:100) as a function of the reciprocal space velocity at 500°C. C_2H_6:O_2 = 3:1.

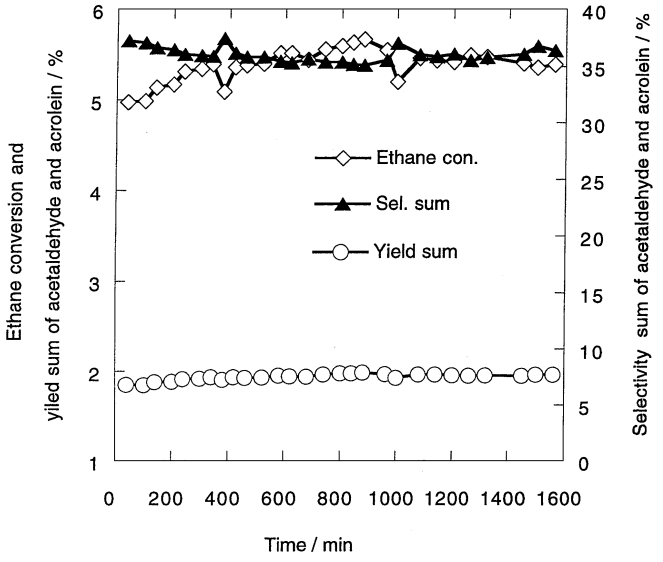

FIG. 4. Catalytic performance of Cs–V/SiO_2 (Cs:V:Si = 1:0.1:100) as a function of reaction time at 500°C. Space velocity, 3000 ml g^{-1} h^{-1}; C_2H_6:O_2 = 3:1.

the ethene selectivity by 2–3 times was also noticeable with this increase in the conversion. At higher vanadium loadings, the conversion decreased but the ethene selectivity was almost kept constant.

In the case of the catalysts containing cesium (Fig. 5b), even very small vanadium loadings up to 0.1 at.% can clearly enhance the ethane conversion. Although the conversion was increased largely by such small vanadium loadings, the aldehyde selectivity was kept around 50%, leading to a large enhancement of the aldehyde yield. A further increase in the vanadium loading brought about a decrease in the aldehyde selectivity and an increase in the CO_x selectivity. The maximum conversion was obseved at a vanadium loading of 2 at.%.

Figure 6 shows the total aldehyde selectivity as a function of the ethane conversion. Different ethane conversions were obtained by changing the reaction temperature as in Fig. 2. The aldehyde selectivity of Cs–V/SiO_2 with different vanadium loadings can be compared under same conversion of ethane. The catalysts supporting a very small amount of vanadium (0.02, 0.05, and 0.1 at.%) show similar aldehyde selectivities which are obviously higher than that of the Cs/SiO_2 catalyst without vanadium.

3.3. Oxidation of C2 and C3 Hydrocarbon over V/SiO_2 (0.1:100) and Cs–V/SiO_2 (1:0.1:100) in the Oxidation of C_2H_6, C_2H_4, C_3H_8, and C_3H_6

The oxidations of C2 and C3 alkane and alkene were compared on the V/SiO_2 (0.1:100) and the Cs–V/SiO_2 (1:0.1:100) catalysts and the results are listed in Table 2. The addition of Cs to the V/SiO_2 catalyst enhanced the ethane conversion and the aldehyde selectivity over ethane, as shown in Figs. 1 and 2. At the same time, the distribution of produced aldehydes changed, where an increase in the selectivity for aldehyde with higher carbon numbers was induced by the Cs addition. Similar effects of Cs were also observed in the case of propane oxidation. It is also noteworthy that the alkane reactivity on the Cs-containing catalyst is higher than that of alkene, though the alkene reactivity on the Cs-free catalyst is much higher than the alkane reactivity. A larger quantity of aldehydes was produced from alkane than from alkene over the Cs-containing catalyst.

Ethanol, as well as ethene, is a possible intermediate from ethane to aldehydes. The oxidation of ethanol vapor was examined on the V/SiO_2 (0.1:100) and the Cs–V/SiO_2 (1:0.1:100) catalysts and results are shown in

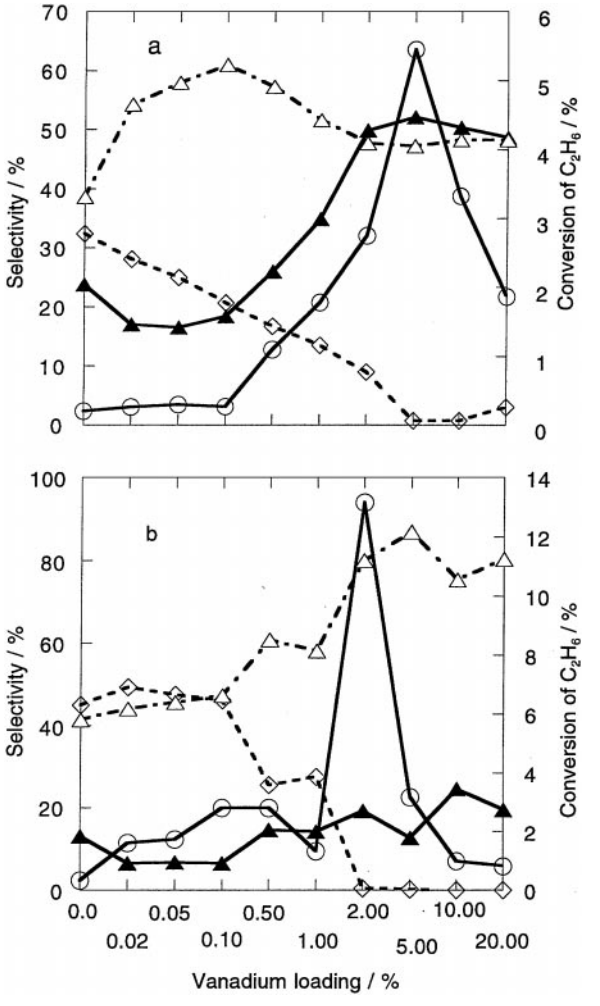

FIG. 5. Effect of vanadium loading amount on the product distribution and ethane conversion over V/SiO_2 (V:Si = *x*:100) (a) and Cs–V/SiO_2 (Cs:V:Si = 1:*x*:100) (b). Reaction temperature, 475°C; space velocity, 3000 ml g^{-1} h^{-1}; C_2H_6:O_2 = 3:1. Key: ○, C_2H_6 Con; ◇, total S to oxygenates; ▲, C_2H_4 selectivity; △, CO_x selectivity.

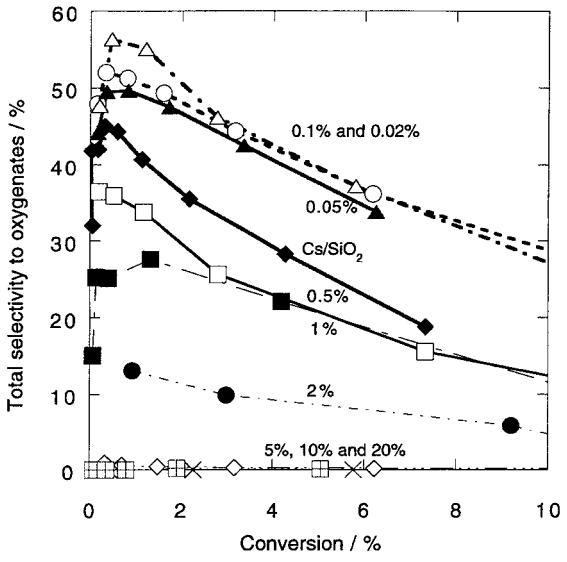

FIG. 6. Effect of vanadium loading amount on the total selectivity for aldehydes over Cs–V/SiO_2 (Cs:V:Si = 1:*x*:100) as a function of ethane conversion. Space velocity, 3000 ml g^{-1} h^{-1}; C_2H_6:O_2 = 3:1; reaction temperatures, 400–600°C.

Table 3. Acetaldehyde was obtained through ethanol oxidation on both V/SiO_2 and Cs–V/SiO_2. Cs addition to V/SiO_2 reduced the formaldehyde selectivity and enhanced the acrolein selectivity. With increasing temperatures, i.e., increasing conversions, the acetaldehyde selectivity decreased and the acrolein selectivity increased on Cs–V/SiO_2. The ethene selectivity observed here was higher than those observed in ethane oxidation over the same catalysts.

3.4. Specific Surface Area, Colors, and Absorption Spectra

The BET specific surface areas and colors of the V/SiO_2 and Cs–V/SiO_2 catalysts are summarized in Table 4. The number of VO_x per square nanometer on the silica surface, which was simply calculated by dividing the vanadium loading by the surface area of the samples, is also shown in Table 4.

In the V/SiO_2 samples, a slight decrease in the surface area of silica (originally about 400 m^2/g) was observed when the vanadium loadings were less than 2 at.%. The surface area of V/SiO_2 suddenly decreased when the vanadium loading exceeded 5 at.%. Such a sudden decrease in the surface area with increasing vanadium loading was also observed in the Cs–V/SiO_2 samples supporting vanadium at more than 2 at.%, even though the surface area of the samples with lower vanadium loading was reduced by cesium addition down to about 50%.

Diffraction analysis by X-ray (XRD) has been attempted for all the samples listed in Table 4. There was, however, no diffraction peak, except for the V/SiO_2 (20:100) sample that showed very weak diffraction pattern originating from V_2O_5.

The absorption spectra of V/SiO_2 and Cs–V/SiO_2 were measured in the UV–vis region and the results are shown in Fig. 7. One absorption edge and three absorption bands were observed: absorption edge A1 in the wavelength region of 600–700 nm, absorption band A2 in the region of 400–600 nm, A3 band centered at about 330 nm, and A4 band centered around 265 nm. The UV–vis absorptions of vanadium oxide species, except A4, have already been discussed and assigned in previous literature. The reported assignments are listed in Table 5. There are very few discussions about the A4 band, which is often accompanied with A3 in the spectra (32).

The samples with high vanadium loadings (>5 at.%) showed the A1 absorption edge. The absorption band A2 was seen in the V/SiO_2 samples of V > 0.1 at.% and the Cs–V/SiO_2 samples of V > 1 at.%. The A3 and A4 bands seem to overlap in all the absorption spectra shown in Fig. 7. However, the samples of V < 0.1 at.% showed a clear doublet of A3 and A4.

Although the absorbance shown here is in arbitrary units, the relative absorbance of V/SiO_2 was higher than that of Cs–V/SiO_2. In both cases, a decrease in absorbance was

TABLE 2

Catalytic Performance of V/SiO_2 (V:Si = 0.1:100) and Cs–V/SiO_2 (Cs:V:Si = 1:0.1:100) in the Oxidation of Ethane, Ethene, Propane, and Propene at 475°C

Sample	Substrate	Conv. (%)	Selectivity (%)								
			HCHO	CH_3CHO	CH_2=CHCHO	CH_3COCH_3	C_2H_4	C_2H_6	C_3H_6	CO_x	Total aldehydes
V/SiO_2	C_2H_6	0.3	8.0	12.6	0.0	0.0	18.4		0.0	61.0	20.6
	C_2H_4	1.2	8.4	8.5	1.7	0.0		0.0	0.3	81.1	18.6
	C_3H_8	0.6	6.1	6.2	10.7	8.1	0.0	0.0	0.0	68.9	31.1
	C_3H_6	2.4	7.0	16.8	30.2	9.0	0.2	0.0		36.8	63.0
Cs–V/SiO_2	C_2H_6	2.8	1.6	29.9	14.7	0.0	6.5		0.0	47.3	46.2
	C_2H_4	0.8	13.0	4.0	10.1	0.0		0.0	0.4	72.5	27.1
	C_3H_8	1.1	n.d.	9.3	18.0	34.6	0.0	2.3	0.0	35.8	61.9
	C_3H_6	0.9	n.d.	17.5	32.3	6.0	0.1	0.0		44.1	55.8

TABLE 3

Catalytic Performance of V/SiO_2 (V:Si = 0.1:100) and $Cs–V/SiO_2$ (Cs:V:Si = 1:0.1:100) in Ethanol Oxidation

Reaction temp. (°C)	Sample	C_2H_5OH conv. (%)	Selectivity (%)							
			HCHO	CH_3CHO	CH_2=CHCHO	CH_4	C_2H_4	C_3H_6	C_3H_8	CO_x
300	V/SiO_2	9.0	1.1	51.3	0.0	1.0	39.5	0.0	0.4	6.7
	$Cs–V/SiO_2$	5.6	0.4	73.5	0.0	3.1	3.1	0.0	0.0	19.9
350	V/SiO_2	82.7	3.7	36.8	0.4	0.8	45.8	0.0	1.1	11.4
	$Cs–V/SiO_2$	27.8	2.4	66.5	3.8	1.5	6.0	0.0	0.3	19.5
400	V/SiO_2	99.9	5.6	26.2	4.5	1.4	37.1	0.2	0.7	24.3
	$Cs–V/SiO_2$	96.6	1.1	24.2	11.8	1.6	12.8	0.1	0.0	48.4
450	V/SiO_2	100	8.2	11.6	3.4	1.9	36.4	0.4	0.5	37.6
	$Cs–V/SiO_2$	99.9	1.7	7.3	12.3	2.5	21.6	0.1	0.0	54.5

observed at higher vanadium loadings (V > 10 at.% for V/SiO_2 and V > 5 at.% fro $Cs–V/SiO_2$).

The transmittance of V/SiO_2 and $Cs–V/SiO_2$ was measured in the IR region and results are shown in Figs. 8 and 9, respectively. The spectrum of SiO_2 (top trace in Fig. 8) exhibits a flat and broad absorption band in the region of 1050–1250 cm^{-1}, as well as intensive absorption bands at 815, 1375, 1630, 1870, and 2325 cm^{-1}. This spectrum of SiO_2 is in agreement with that reported by Wokaun *et al.* (41). The peaks higher than 1300 cm^{-1} appear in all the silica-supported samples and remain unchanged in frequency.

For comparison, Fig. 8 includes the spectrum of the sample VO_x which was obtained by thermal decomposition of ammonium vanadate at 600°C, similar to the V/SiO_2 preparation. The spectrum (the bottom trace in Fig. 8) exhibits two small and sharp bands at 425 and 460 cm^{-1}, one broad band from 500 to 650 cm^{-1}, as well as bands at 820, 1020, 1120, 1380, 1625, 1985, and 2310 cm^{-1}. The bands at 820, 1020, and 500–650 cm^{-1} are attributed to the vibrations from V_2O_5 (41, 42), indicating that V_2O_5 is the main component of the VO_x sample.

It is noticeable that three kinds of absorption vary with the extent of loading of vanadium on silica: absorption peaks at 480 and 950 cm^{-1}, and a small absorption shoulder at 1000 cm^{-1}.

The band at 1020 cm^{-1}, which is one of the characteristic bands of V_2O_5 related to the vibration of terminal V=O, disappears on samples with high loadings of vanadium (20% and 10%).

A new and strong band at 940 cm^{-1} appears for the two samples, which is associated with $\nu_{V=O}$ from a VO_x "cluster" (43–45), indicating that some amount of VO_x "cluster" formed in the samples with high loading of vanadium (20%, 10%).

Based on the frequencies, these clusters may correspond to tetrahedral dioxo species (46–48). The intensity of the absorbance band at 940 cm^{-1} in the spectrum of the sample with 20% loading is higher than that of the sample with 10% loading.

The band at 940 cm^{-1} vanishes and a small shoulder peak at 975 cm^{-1} can be observed in the spectra of samples with medium or low loading of vanadium (5, 1, 0.5, and 0.1%). The band at 975 cm^{-1} was characterized as $\nu_{V=O}$ from monomeric vanadyl hydrate species (41, 43).

In the absence of water, the monomeric structure is characterized by a vibration band at 1030–1049 cm^{-1}. When

TABLE 4

Surface Areas and Colors of V/SiO_2 (V:Si = *x*:100, in Molar Ratio) and $Cs–V/SiO_2$ (Cs:V:Si = 1:*x*:100)

V loading (%)	Color		Surface area (m^2/g)		Number of VO_x (nm^{-2})	
	V/SiO_2 (*x*:100)	$Cs–V/SiO_2$ (Cs:V:Si = 1: *x*:100)	V/SiO_2	$Cs–V/SiO_2$	V/SiO_2	$Cs–V/SiO_2$
0.00	white	white	396	200	—	—
0.02	white	white	353	223	0.006	0.009
0.05	white	white	414	219	0.012	0.023
0.10	light yellow	white	388	158	0.026	0.062
0.50	orange	white	350	203	0.140	0.240
1.0	brick red	light yellow	354	198	0.280	0.490
2.0	brick red	yellow	346	108	0.580	1.83
5.0	deep brick red	brown	203	27.0	2.49	18.2
10.0	yellowish brown	brown	47.3	10.0	21.5	99.8
20.0	yellowish brown	brown	14.6	6.3	142	320

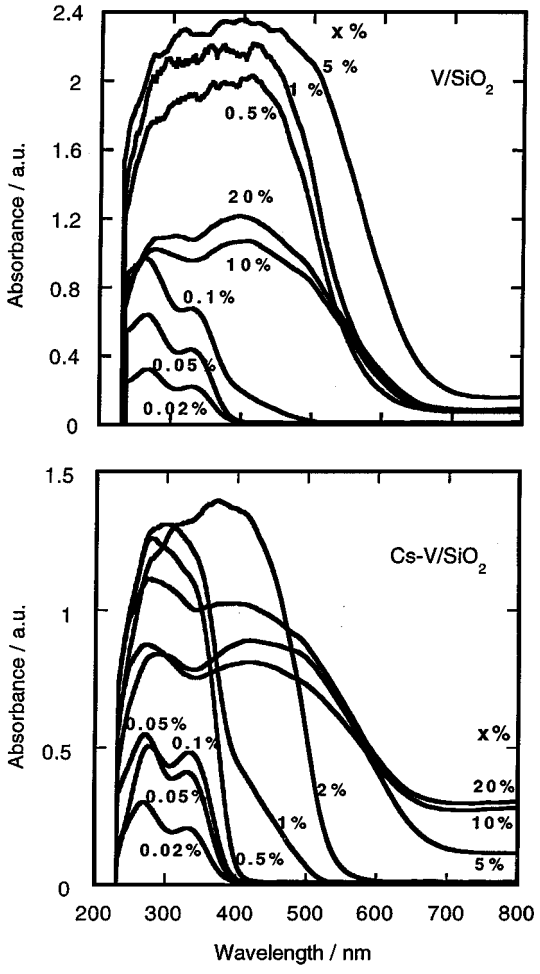

FIG. 7. UV–visible spectra of V/SiO_2 (V:Si = *x*:100) and Cs–V/SiO_2 (Cs:V:Si = 1:*x*:100).

water vapor is present a broad peak in the vicinity of 900–1000 cm^{-1} is observed, which is attributed to hydrated vanadyl groups (43, 49). In our case, the disk was prepared in air. Thus, some water was absorbed by SiO_2 supporting samples.

TABLE 5

Assignment of the Absorption by Vanadium Oxide Species in the UV–Visible Region

	λ/nm	Assignment	Ref.
A1	600–800	d–d transition of V^{4+} in a distorted octahedral symmetry	28
A2	400–600	polymeric vanadate with an energy band structure similar with V_2O_5	29, 30
		V^{5+} in octahedral environment	23, 31
A3	330	V^{5+} in a tetrahedral environment, isolated vanadyl species	19, 20, 30, 32, 33, 34
A5	380–420	polymeric vanadate, V^{5+} in tetrahedral environment	32, 33, 34

Table 6 shows the correlation between V=O vibration frenquecies and the number of terminal V=O group per vanadium (19, 49). The vibration frequency decreases with the increasing number of terminal V=O. The bottom data in Table 3 are our results from this study. Therefore, the structure of the vanadyl species is monoxo vanadyl.

The variable trend of FT-IR spectra of samples with cesium is very similar to that of samples without cesium. However, there is one difference: the band at 940 cm^{-1} does not appear in the spectrum of V/SiO_2 (5%) while a very clear

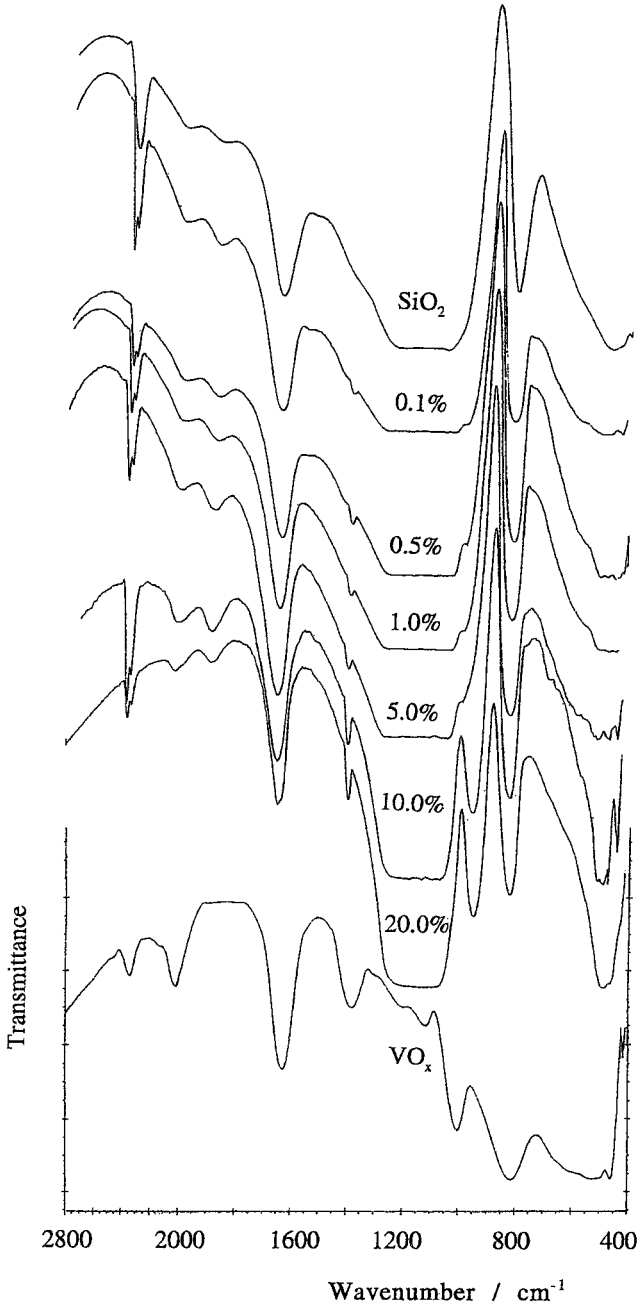

FIG. 8. FT-IR spectra of V/SiO_2 (V:Si = *x*:100, *x* = 0.0, 0.1, 0.5, 1.0, 5.0, 10.0, and 20.0).

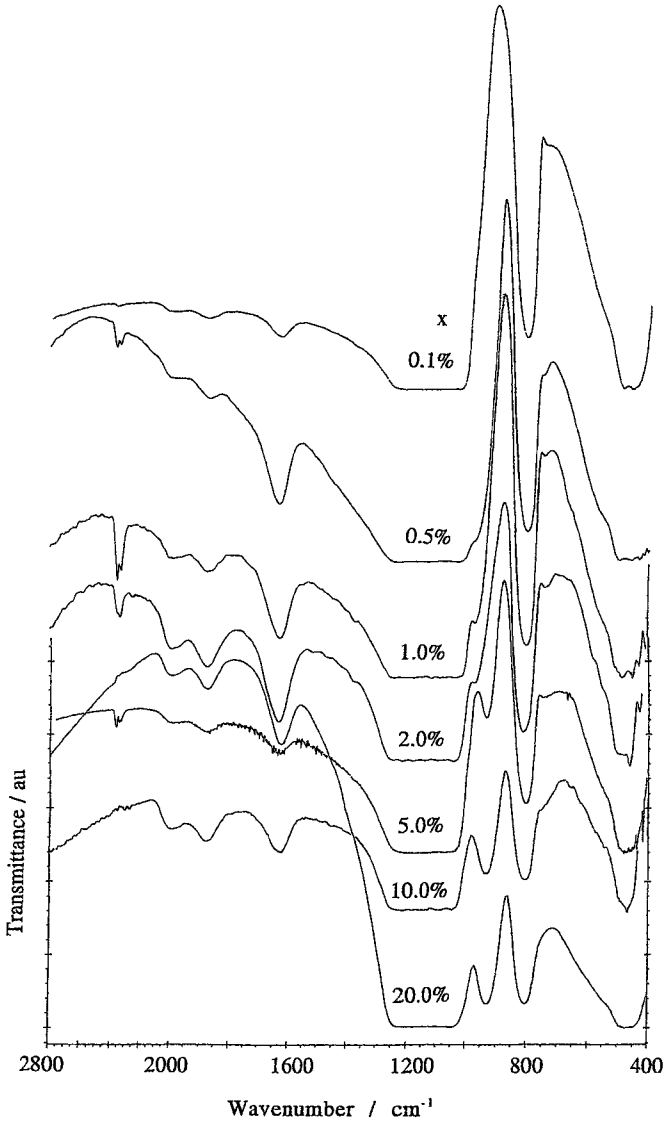

FIG. 9. FT-IR spectra of Cs–V/SiO_2 (Cs:V:Si = 1:*x*:100, $x = 0.0$, 0.1, 0.5, 1.0, 2.0, 5.0, 10.0, and 20.0).

band appears in the spectrum of Cs–V/SiO_2 (5%), indicating that the presence of cesium promotes the formation of cluster with dioxo tetrahedral coordination.

Electron spin resonance was used to gain information to determine whether the samples contain some amount of V^{4+} species. All the samples were measured at liquid nitrogen temperature. No ESR signals of V^{4+} were observed in the samples whose vanadium loading was lower than 5% both in the absence and in the presence of cesium. This indicates that either there is no V^{4+} species existing in these samples or there is too small an amount of V^{4+} to be detected by ESR.

TABLE 6

V=O Vibration Frequencies as a Function of Number of V=O per Vanadium (19, 45)

Species	γ (cm^{-1})	V=O groups/V atom
$[VO_4]^{3-}$	827–850	4
$V_2O_7^{4-}$	873–912	3
$[(VO_3)_n]^{n-}$	927–950	2
$[VO_4]^{3-}$	975	1

4. DISCUSSION

4.1. Vanadium Species on the Catalysts with Different Vanadium Loadings with and without Cesium

Three types of catalytic properties, oxidative dehydrogenation, aldehyde formation, and combustion, were found in the V/SiO_2 and Cs–V/SiO_2 systems during the oxidation of ethane by oxygen. Before the discussion of the activity and the selectivity, dominant surface species on the V/SiO_2 and Cs–V/SiO_2 catalysts are considered.

Crystal V_2O_5 is not the main component of the vanadium species in the high-V-loading catalysts (V = 5–20 at.%). Only V/SiO_2 (V = 20 at.%) catalyst gave the very weak V_2O_5 pattern of XRD. In addition, the IR patterns of the high-loading samples were different from that of V_2O_5. The sudden decrease in the surface area at high loadings (V > 5 at.% for V/SiO_2 and V > 2 at.% for Cs–V/SiO_2) suggests that vanadium oxide is three-dimensionally grown in the micropore of the silica support. The IR absorption at 940 cm^{-1} indicates the presence of a VO_x "cluster" (43–45) with tetrahedral dioxo species (46–48). The difference in the relative absorbances in the UV–vis spectra can be related to the change in the surface area, where the samples with lower surface area (especially for higher V-loadings) show relatively weak UV–vis absorbances. Scattering of the UV–vis light might be affected by the microstructure of the samples.

The number of VO_x per square nanometer of surface of about 2.0 has been proposed as one characteristic of monolayer structure (23) for the supported vanadium catalysts. Such a VO_x density corresponds to the V/SiO_2 (V = 5 at.%) catalyst and the Cs–V/SiO_2 (V = 2 at.%) catalyst, as shown in Table 4. It is not contradictory that the filling of micropores of the silica with the VO_x clusters is estimated to begin around these vanadium loadings, according to the decrease of the surface area with increasing V loadings. The lower vanadium loading required for the monolayer structure of the Cs-containing sample can be explained if the smaller surface area of these samples is taken into account. The surface structure of silica is essentially sensitive to alkali.

Although the IR absorption at 975 cm^{-1} suggests the presence of monomeric vanadyl hydrate species (41, 43) in the middle V-loading region (V = 0.1–5 at.% and 1–2 at.% for the catalysts with and without Cs, respectively), it is evident from the UV–vis spectrum (A3 absorption)

that polymeric vanadate species (28, 29) still exist. The surface of silica is estimated not to be fully covered with vanadium species in this middle loading region.

Domain size of semiconductive microcrystallites can be estimated from the blue shift of the band-gap absorption (quantum size effect) (35–47) and this method is also available for the size estimation of the supported catalysts (38, 39) Khodakov *et al.* (21, 22) determined the domain size changes in several systems of vanadium-supported catalyst by this method to characterize the charge-transfer transition at the absorption in the UV–vis spectra, which was defined as the first inflection point in the Kubelka–Munk function. Very recently, Barton *et al.* (40) refined the treatment by taking into account the actual nature of the electronic transitions.

Although no semiconductive crystallites but several vanadium species are estimated to exist in the present catalysts, the absorption edge energy was calculated according to the reported method (21, 40). Figure 10 shows the absorption edge energy as a function of the surface density of vanadium. A constant absorption edge energy of 1.8 eV, which is similar to the band gap energy of V_2O_5 (2.05 eV) (22), was observed at a high vanadium density. With decreasing V density, a high-energy shift (or blue-shift) of the absorption becomes distinct (quantum size effect). It is noteworthy that the presence of Cs greatly affects the beginning of the blue shift. If a V density of about 2.0 nm^{-2} is assumed as the monolayer quantity of vanadium, the blue shift with decreasing V density starts at V density higher than the monolayer quantity on the Cs-containing samples but at V density lower than the monolayer quantity on the Cs-free

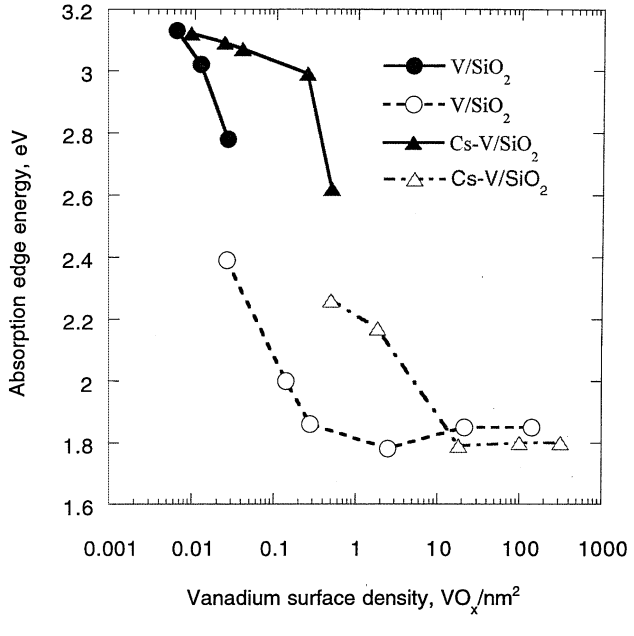

FIG. 10. Dependence of UV–visible absorption edge energy on the VO_x surface density.

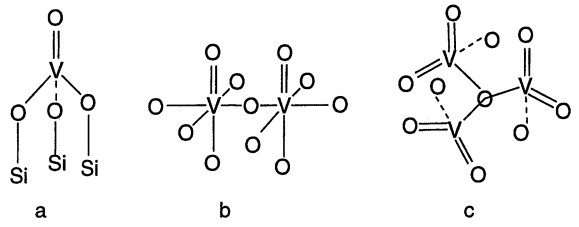

FIG. 11. Proposed structures of vanadyl species.

samples. This indicates that Cs can induce vanadium species with smaller domain size: smaller three-dimensional clusters or, more plausibly, two-dimensional islands on silica.

At lower V loadings, an independent absorption band (A3) appeared and the absorption edge energy converged to around 3.1 eV. This is indicative of the isolated V^{5+} in a tetrahedral environment (21, 22, 33, 34). The transformation from the A2 absorption to the A3 absorption appears at higher V loadings (V = 0.5 nm^{-2} or 1 at.%) for Cs–V/SiO_2 than for V/SiO_2 (V = 0.03 nm^{-2} or 0.1 at.%). These facts suggest that Cs can stabilize the V–O–Si structure rather than the V–O–V structure and is effective for the dispersion of vanadium species on silica.

To summarize the characterization of vanadium species in the present catalysts, following species were estimated: (i) for V/SiO_2 with V > 5 at.% and Cs–V/SiO_2 with V > 2 at.%, three-dimensionally grown clusters and vanadium–oxygen clusters with dioxo tetrahedral coordination states; (ii) for V/SiO_2 with V = 0.1–5 at.% and Cs–V/SiO_2 with V = 1–2 at.%, two-dimensional polymeric vanadyl species with octahedral coordination; and (iii) for V/SiO_2 with V < 0.1 at.% and Cs–V/SiO_2 with V < 1 at.%, isolated species with tetrahedral coordination. Although Cs seems to affect the morphology of the vanadium species on silica, no direct evidence for the formation of particular species consisting of V and Cs was observed at present. The possible structures of these three types of vanadyl species are shown in Figs. 11a, 11b, and 11c, respectively.

4.2. Dependence of the Activity and the Product Selectivity on the Catalyst Composition

When Cs was not added to the catalysts, pure silica and silica-supported vanadium gave aldehydes with small selectivities, and ODH of ethane to ethene took place selectively on the silica with medium and high V loadings. These facts are consistent with the results of Oyama and Somorjai (6, 7), and are also not contradictory to the reports on the vanadium-catalyzed ODH of propane by Khodakov *et al.* (21, 22).

The dependence of the ethene selectivity on the V loading (Fig. 5a) suggests that the ethene selectivity increases linearly with an increase in the vanadium coverage of the surface. Here, the V–O–V structure rather than isolated V

species is considered to be more important for the ethane ODH. This is because the V/SiO_2 (V = 0.1 at.%) catalyst, the main component of which is the isolated V species (Fig. 7), shows almost the same ethene selectivity and the same ethane conversion as pure silica shows. However, the V/SiO_2 (V = 0.5 at.%) catalyst, the main component of which is a polymeric one, affords the distinct enhancement in the ethene selectivity as well as a higher conversion than that of pure silica.

Apparent maximum conversions of ethane can be seen on both the V/SiO_2 and $Cs–V/SiO_2$ catalysts with V loadings corresponding to the monolayer quantity (Fig. 5). This might not be due to the chemical origin, because the surface area seriously decreases at V loadings higher than the monolayer quantity. In addition, the product selectivities at higher V loadings are almost kept constant. Figure 12 shows the relative reaction rate normalized to the number of VO_x supported on silica as a function of the vanadium surface density (21, 22). It is clear that no peculiar activity was observed around the monolayer quantity of vanadium (about 2.0 nm^{-2}) (23). Both the two-dimensional island species (medium loading) and three-dimensionally grown clusters of vanadium species (high loading) might show, thus, similar specific catalysis toward the ethane ODH.

The normalized rate, $(1–5) \times 10^{-3}$ s^{-1}, of ethane oxidation over the present V/SiO_2 catalysts (Fig. 12) does not differ much from the TOF listed in Table 1. However, a very high normalized rate can be seen on the $Cs–V/SiO_2$ catalysts with V density lower than 0.1 nm^{-2}. These high-rate catalysts ($Cs–V/SiO_2$ with V = 0.02, 0.05, and 0.1 at.%)

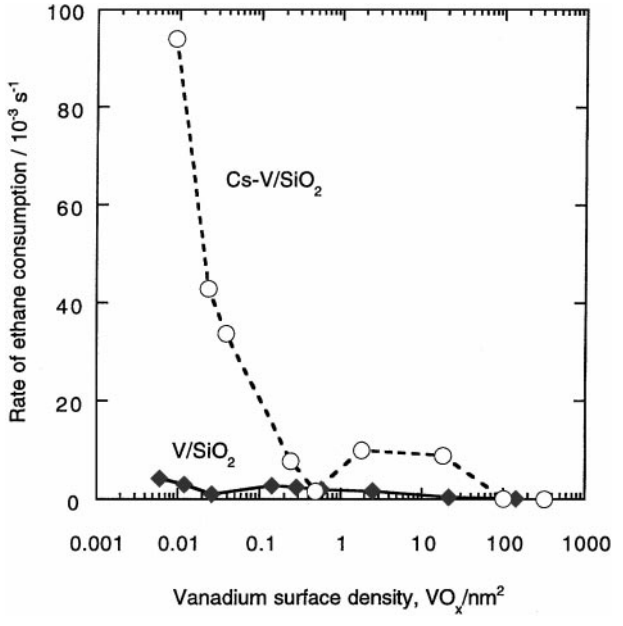

FIG. 12. Dependence of ethane consumption rate on VO_x surface density. Reaction temperature, 475°C; space velocity, 3000 ml g^{-1} h^{-1}; C_2H_6:O_2 = 3:1.

afforded, at the same time, a high aldehyde yield (Fig. 6) and were estimated to consist of only isolated vanadium species (Fig. 7b). The aldehyde yield of about 3% obtained in the present study is much higher than those reported in the ethane–oxygen reaction and is also comparable to the highest yield in the ethane–N_2O reaction (Table 1). The V/SiO_2 catalysts with V = 0.02 and 0.05 at.%, which were also estimated to consist of only isolated vanadium species (Fig. 7a), did not show a high reaction rate nor a high aldehyde yield. Therefore, the importance of the combination between Cs and isolated vanadium species on silica becomes prominent for the high aldehyde yield. Yoshida *et al.* (50) have pointed out the importance of the combination between alkali and distorted tetrahedral vanadium species on silica for the photooxidation of propane into oxygenates. By contrast, the interaction of Cs with two-dimensional polymeric vanadyl species (medium loading) or three-dimensionally grown clusters of VO_x (high loading) diminishes their ODH catalysis but brings about the combustion ability. Compounds including Cs and V might be formed as the active species, though no evidence is available for this at present.

4.3. Reaction Pathways for the Production of Acrolein

During the course of the aldehyde formation over the $Cs–V/SiO_2$ catalysts with low V loadings, a considerable amount of acrolein was detected. The dependence of the aldehyde selectivity on the contact time, as shown in Fig. 3, suggests that the formations of acetaldehyde and formaldehyde take place at an early stage of the reaction and they are succeeded by the acrolien formation.

Three possible routes can be considered for the acrolein formation: [1] a cross-aldol-condensation between acetaldehyde and formaldehyde (51, 52), [2] the cracking of C4 aldehydes produced through self-condensation of acetaldehyde (52), and [3] the selective oxidation of propane or propene produced from ethane:

$$\begin{aligned} CH_3CHO + HCHO &\rightarrow CH_2(OH)CH_2CHO \\ &\rightarrow CH_2{=}CHCHO + H_2O \end{aligned} \quad [1]$$

$$\begin{aligned} 2CH_3CHO &\rightarrow CH_3CH{=}CHCHO \\ &\rightarrow CH_2{=}CHCHO + \text{C1 products} \end{aligned} \quad [2]$$

$$C_2H_6 \rightarrow C_3H_8 \quad \text{or} \quad C_3H_6 \rightarrow CH_2{=}CHCHO \quad [3]$$

No C4 aldehyde was detected in the present ethane oxidation. In addition to this, the self-condensation of acetaldehyde was not observed when acetaldehyde vapor was passed over the $Cs–V/SiO_2$ catalysts. Therefore, acrolein formation via Eq. [2] can be excluded from the possible reaction routes. It is well known that acrolein is produced by selective oxidation of propene or propane. Indeed, acrolein

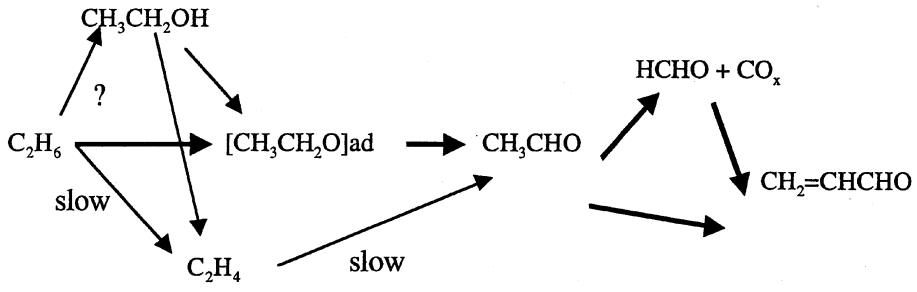

SCHEME 1. Proposed reaction pathways from ethane to acrolein.

was formed in the oxidation of propene or propane over the Cs–V/SiO_2 catalyst (Table 2). It is noticed that an appreciable amount of acetone is also formed in the propene or propane oxidation. During ethane oxidation on the Cs–V/SiO_2 catalyst, no acetone was detected. Moreover, neither propene nor propane from ethane was observed at reaction temperatures below 500°C. The reaction route of Eq. [3] can also be neglected. Consequently, the cross-condensation represented by Eq. [1] is regarded as the most plausible route for acrolein formation. This pathway proposed here is consistent with the dependence of the aldehyde selectivity on the contact time, as shown in Fig. 3. Alkali has been reported to catalyze the cross-condensation between acetaldehyde and formaldehyde (51, 52).

As for acetaldehyde formation, ethene and ethanol are possible intermediates from ethane. The reactivity of ethene on Cs–V/SiO_2 is much lower than that of ethane (Table 2). In addition, the distributions of the products from ethane and ethene are different. In the ethene oxidation, the formaldehyde and CO_x selectivities are higher but the acrolein selectivity is lower than those from ethane. Therefore, it is hard to consider ethene as an intermediate from ethane to acetaldehyde.

The aldehyde distribution in ethanol oxidation and the change of the aldehyde selectivities with changing conversion over Cs–V/SiO_2 (Table 3) are similar to those observed in ethane oxidation. Although ethanol is not detected in ethane oxidation and the ethene selectivity from ethanol is higher than that from ethane, the observed similarity in aldehyde formations from ethane and ethanol suggests that a common reaction step might be included, at least, in these two pathways giving acetaldehyde.

Based on the discussion above, the possible reaction pathways over the Cs–V/SiO_2 catalyst are proposed as shown in Scheme 1.

4.4. Role of Cesium

Several effects of Cs were observed in the present study. The change in the morphology of vanadium species by Cs has been discussed in Section 4.1. Other catalytic effects are summarized as follows:

(1) The addition of Cs to the low-V-loading catalysts enhances the reaction rate by about 50 times (Fig. 12).

(2) The addition of Cs to the low-V-loading catalysts enhances the alkane reactivity but reduces the alkene reactivity (Table 2).

(3) The addition of Cs to the low-V-loading catalysts enhances the selectivity for acetaldehyde and acrolein but reduces the formaldehyde selectivity, leading to a higher selectivity for total aldehydes.

(4) The addition of Cs to the medium- and high-V-loading catalysts enhances their combustion ability and reduces the catalysis of ODH.

Qualitatively the same effects of Cs (or alkali) have been reported in the propane oxidation on K–Fe/SiO_2 (26, 27). Neutralization of acid sites by Cs might be effective for the prevention of the acid-catalyzed scission of C–C bonds. Alkali can catalyze the cross-condensation between acetaldehyde and formaldehyde, as discussed above. These two roles of Cs (or alkali) are considered to be related to the modification of aldehyde selectivities (26, 27). Although a repulsive interaction between π-electrons in alkenes and the basic surface of catalysts (26, 27, 53) may partly explain the modification of activities, further studies are required to interpret all the functions of Cs in the oxidation of ethane by oxygen.

5. CONCLUSIONS

Silica-supported vanadium with very low loadings of vanadium (V:Si = 0.02–0.1 at.%) and cesium (Cs:Si = 1at.%) was found to give acrolein as well as acetaldehyde in the oxidation of ethane by oxygen, while the low-V-loading catalysts without Cs showed a much lower catalytic activity. Isolated vanadyl species with tetrahedral coordination were estimated to be the active species for aldehyde formation with a relatively high normalized rate through the interaction with cesium. Cesium-catalyzed cross-condensation between acetaldehyde and formaldehyde was also proposed for the formation of acrolein from ethane. Neutralization of acid sites by Cs^+ might be effective for the suppression of C–C bond-breaking, which leads to the

decomposition and then the high level of oxidation of hydrocarbons.

The ODH of ethane was observed over silica with medium and high vanadium loadings (V:Si = 0.5–20 at.%) if Cs was not added. Two-dimensional polymeric vanadyl species with octahedral coordination and three-dimensional vanadium–oxygen clusters with dioxo tetrahedral coordination were detected in the samples with medium (0.5–5.0 at.%) and high (10 and 20 at.%) vanadium loadings, respectively. The catalysis of the ODH can be attributed to both of these species. The apparent high ethane conversions observed on the catalysts covered with about a monolayer of vanadium were not due to the chemical origin, but are simply explainable on the basis of the change in the specific surface area. Normalized rates on these species were not very different.

Addition of cesium to the polymeric vanadyl species with octahedral coordination and the vanadium–oxygen clusters with dioxo tetrahedral coordination altered their catalysis from ODH to combustion. The formation of alkali vanadates was not detected. The reason for the high CO_x selectivity on these catalysts is not clear at present.

ACKNOWLEDGMENT

This work was supported by New Energy and Industrial Technology Development Organization (NEDO).

REFERENCES

1. Albonetti, S., Cavani, F., and Trifiro, F., *Catal. Rev. Sci. Eng.* 413 (1996).
2. Owens, L., and Kung, H., *J. Catal.* **144**, 202 (1993).
3. Bettahar, M. M., Costentin, G., Savary, L., and Lavalley, J. C., *Appl. Catal. A* **145**, 1 (1996).
4. Mamedov, E. A., and Corberan, V. C., *Appl. Catal. A* **127**, 1 (1995).
5. Iwamoto, M., Taga, T., and Kagawa, S., *Chem. Lett.* 1469 (1982).
6. Oyama, S. T., and Somorjai, G. A., *J. Phys. Chem.* **94**, 5022 (1990).
7. Oyama, S. T., *J. Catal.* **128**, 210 (1991).
8. Mendelovici, L., and Lunsford, J. H., *J. Catal.* **94**, 37 (1985).
9. Erdohelyi, A., and Solymosi, F., *Appl. Catal.* **39**, L11 (1988).
10. Erdohelyi, A., and Solymosi, F., *J. Catal.* **123**, 31 (1990).
11. Erdohelyi, A., and Solymosi, F., *Catal. Lett.* **8**, 229 (1991).
12. Erdohelyi, A., and Solymosi, F., *J. Catal.* **129**, 497 (1991).
13. Erdohelyi, A., and Solymosi, F., *J. Catal.* **135**, 563 (1992).
14. Erdohelyi, A., Cserenyi, J., and Solymosi, F., *ACS Symp. Ser.* **523**, 368 (1993).
15. Andersen, P. J., and Kung, H. H., *in* "New Frontiers in Catalysis" (L. Guczi, F. Solymosi, and P. Tetenyi, Eds.), p. 205. Elsevier Science, Amsterdam, 1993.
16. LeBars, J., Vedrine, J. C., Auroux, A., Trautmann, S., and Baerns, M., *Appl. Catal. A* **88**, 179 (1992).
17. Centi, G., Perathoner, S., Trifiro, F., Aboukais, A., Aissi, C. F., and Guelton, M., *J. Phys. Chem.* **96**, 2617 (1992).
18. Bellussi, G., Centi, G., Perathoner, S., and Trifiro, F., *in* "Catalytic Selective Oxidation" (S. T. Oyama and J. W. Hightower, Eds.), p. 281. American Chemical Society, Washington DC, 1992.
19. Eon, J. G., Olier, R., and Volta, J. C., *J. Catal.* **145**, 318 (1994).
20. Blasco, T., Galli, A., Nieto, J. M. L., and Trifiro, F., *J. Catal.* **169**, 203 (1997).
21. Khodakov, A., Yang, J., Su, S., Iglesia, E., and Bell, A. T., *J. Catal.* **177**, 343 (1998).
22. Khodakov, A., Olthof, B., Bell, A. T., and Iglesia, E., *J. Catal.* **181**, 205 (1999).
23. Wachs, I. E., and Weckhuysen, B. M., *Appl. Catal. A* **157**, 67 (1997).
24. Kobayashi, T., Nakagawa, K., Tabata, K., and Haruta, M., *J. Chem. Soc., Chem. Commun.* 1609 (1994).
25. Kobayashi, T., Guihaume, N., Miki, J., Kitamura, N., and Haruta, M., *Catal. Today* **32**, 171 (1996).
26. Teng, Y., and Kobayashi, T., *Chem. Lett.* 327 (1998).
27. Teng, Y., and Kobayashi, T., *Catal. Lett.* **55**, 33 (1998).
28. Busca, G., Marchetti, L. J., Centi, G., and Trifiro, F., *J. Chem. Soc., Faraday Trans.* **81**, 1003 (1985).
29. Hanke, W., Bienert, R., and Jerschkewitz, H. G., *Z. Anorg. Allg. Chem.* **414**, 109 (1975).
30. Lischke, G., Hanke, W., Bienert, R., Jerschkewitz, H. G., and Ohlmann, G., *J. Catal.* **91**, 54 (1985).
31. Schraml-Marth, M., Wokaun, A., and Baiker, A., *J. Catal.* **130**, 220 (1990).
32. Tanaka, T., Nishimura, Y., Kawasaki, S., Ooe, M., Funabiki, T., and Yoshida, S., *J. Catal.* **118**, 327 (1989).
33. Corma, A., Lopez Nieto, J. M., and Paredes, *Appl. Catal. A* **104**, 161 (1993).
34. Blasco, T., Concepcion, P., Lopez Nieto, J. M., and Perez-Pariente, J., *J. Catal.* **152**, 1 (1995).
35. Cherstnoy, N., Hull, R., and Brugs, L. E., *J. Chem. Phys.* **85**, 2237 (1986).
36. Alivasatos, A. P., *Science* **271**, 933 (1996).
37. Liu, Z., and Davis, R. J., *J. Phys. Chem.* **90**, 2555 (1986).
38. Weber, R. S., *J. Catal.* **151**, 470 (1995).
39. Iglesia, E., Barton, D. G., Soled, S. L., Miseo, S., Baumgartner, J. E., Gates, W. E., Fuentes, G. A., and Meitzner, G. D., *Stud. Surf. Sci. Catal.* **101**, 533 (1996).
40. Barton, D. G., Shtein, M., Wilson, R. D., Soled, S. L., and Iglesia, E., *J. Phys. Chem.* **103**, 630 (1999).
41. Wokaun, A., Schraml, M., and Baiker, A., *J. Catal.* **116**, 595 (1989).
42. Busca, G., and Lavalley, G. C., *Spectrochim. Acta A* **42**, 443 (1986).
43. Cristiani, C., Forzatti, P., and Busca, G., *J. Catal.* **116**, 586 (1989).
44. Griffith, W. P., and Wickins, T. D., *J. Chem. Soc. A* 1066 (1969).
45. Dupuis, T. D., and Lorenzelli, V., *Therm. Anal.* **1**, 15 (1969).
46. Wachs, I. E., Saleh, R. Y., Chan, S. H., and Cherisch, C. C., *Appl. Catal.* **15**, 339 (1985).
47. Kozlowski, R., Pettifer, R. F., and Thomas, J. M., *J. Phys. Chem.* **87**, 5176 (1983).
48. Harber, J., Kozlowska, A., and Kozlowski, R., *J. Catal.* **102**, 52 (1986).
49. Went, G. T., Oyama, S. T., and Bell, A. T., *J. Phys. Chem.* **94**, 4240 (1990).
50. Yoshida, S., Takenaka, S., and Tanaka, T., *Res. Chem. Intermed.* **24**, 309 (1998).
51. Ai, M., *Bull. Chem. Soc. Jpn.* **64**, 1346 (1991).
52. Dumitriu, E., Hulea, V., Chelaru, C., Catrinescu, C., Tichit, D., and Durand, R., *Appl. Catal. A* **178**, 145 (1999).
53. Sokolovskii, V., Arena, F., Giordano, N., and Parmaliana, A., *J. Catal.* **167**, 296 (1997).